bioRxiv preprint doi: https://doi.org/10.1101/810259; this version posted December 20, 2019. The copyright holder for this preprint (which was not certified by peer review) is the author/funder, who has granted bioRxiv a license to display the preprint in perpetuity. It is made available under aCC-BY-NC-ND 4.0 International license.

Metabolic trade-offs expose unforeseen benefits of plasmid carriage

Rafael C. Reding[1]

[1] Living Systems Institute, University of Exeter, Exeter EX4 4QD, UK.

Corresponding author: R.C.Reding-Roman@exeter.ac.uk.

Microbes without plasmids divide faster than those harbouring them. Microbiologists rely on this difference in growth rate between both types of microbe to foresee whether a plasmid will be maintained, or else purged by the host to avoid extinction. However, here I report that plasmids change multiple life-history traits and show that growth rate *alone* can be a bad predictor for plasmid maintenance. Pairwise competition experiments between two constructs of *Escherichia coli*—one of which carries a plasmid—revealed that harbouring plasmids can also increase yield and delay growth (lag). Crucially, yield engaged in a trade-off with growth rate. The plasmid borne by one construct (R), non-transmissible and with a tetracycline-resistance gene, reduced its host's growth rate by 20%. However, given this trade-off, R outgrew its sensitive counterpart (S) in the absence of tetracycline when the competition favoured yield over growth rate. The trade-off makes unclear whether the plasmid is costly to maintain. R-mutants that acquired additional copies of the plasmid, through random segregation, exploited this trade-off and were selected with tetracycline concentrations below the 'minimal selective concentration'—the lowest antimicrobial concentration thought to select for resistant mutants. My data suggests that plasmids interfere with multiple traits, and whether plasmids are costly to maintain will depend on the relationship between them and which is under strongest selection. Thus, concepts that rely on plasmid carriage costs must be used cautiously.

Introduction

Plasmids are independent genetic elements that complement the chromosome of prokaryotes[1,2] and eukaryotes[3] alike. They can benefit cells harbouring them—notoriously in the form of resistance to antibiotics—but the metabolic costs associated with their upkeep can reduce the host's growth rate[2,4]. Clinicians and evolutionary biologists exploit the sensitivity of growth rate to plasmid carriage, using pairwise competition experiments to estimate the costs of plasmid maintenance[5–8] and whether a plasmid will be maintained through time. Their conclusion is straightforward: microbes without plasmids multiply faster in environments where plasmids are not beneficial, and overthrow microbes harbouring them[4,7].

Bacteria, however, can maintain plasmids that have no evident benefit—despite reducing their growth rate[2,9–11]. So, where is the hidden benefit? Plasmids are known to reduce the host's growth rate, but the metabolic alterations that plasmids introduce are unclear[12–15]. Here

bioRxiv preprint doi: https://doi.org/10.1101/810259; this version posted December 20, 2019. The copyright holder for this preprint (which was not certified by peer review) is the author/funder, who has granted bioRxiv a license to display the preprint in perpetuity. It is made available under aCC-BY-NC-ND 4.0 International license.

I asked whether growth rate is the only life-history trait that is sensitive to plasmid carriage, and it is not. I analysed the growth dynamics of two identical constructs[16] of *Escherichia coli*, one of which (R in the remainder) harbours a non-transmissible plasmid with a tetracycline resistance gene, and found that plasmids can also delay the onset of growth (lag) and increment biomass yield. Growth rate and yield engaged in a trade-off that is highly sought after[17–19].

R-cells exploited this trade-off in pairwise competition experiments without tetracycline. The competition favoured yield over growth rate, resulting in R preserving the plasmid—with a tetracycline-resistance gene—for 80< generations. The trade-off between rate and yield has unforeseen consequences beyond plasmid maintenance. The estimation of antimicrobial concentrations that select for drug-resistant mutants—'mutant selection windows'[6]—relies on similar costs, so, how does the above trade-off affect the estimation of selection windows? As I demonstrate below, drug-resistant mutants that exploit this trade-off can be selected below the mutant selection window.

I exposed a mixture of both constructs, S and R, to a range of tetracycline concentrations during a 7-day pairwise competition experiment that favoured yield over growth rate. Without tetracycline R-cells maintained the plasmid with little variation in the number of copies borne, but with antibiotic this number changed: R-cells exposed to more drug hosted more plasmids, even at concentrations below the minimal selective concentration—which defines the lower boundary of the selection window[6]. The gain was detectable within 24h. Mutants harbouring more plasmids had lower yields and shorter lags, but their growth rate increased during the same period. Thus, when plasmids trigger metabolic trade-offs, they can be either costly or beneficial depending on which trait is under selective pressure. Random segregation, commonly associated with plasmid loss in the absence of selection[7], can also explain the accumulation of plasmids in these R-mutants.

Results

Plasmid-mediated trade-off between rate, yield and lag. Growth curves can provide insight into metabolic changes in bacteria. The transition from efficient to inefficient pathways, for example, can be detected analysing them[20,21]. I therefore sought changes in the growth curves (see methods) of two strains of *Escherichia coli* MC4100, one of which, R, bears the plasmid pGW155B[16]. This plasmid contains a tetracycline resistance gene, *tet(36)*, and is non-transmissible, that is, it cannot be transferred horizontally to other cells. Now, the growth curves showed that harbouring pGW155B penalised the growth rate of R by 21.05% ± 2.01% (mean ± standard error with $n = 8$, Mann-Whitney U-test $p = 1.554 \times 10^{-4}$, ranksum = 100) compared to its sensitive counterpart, S, as we may expect (Figure 1A). But they also exposed noteworthy differences in other growth parameters.

Despite their lower growth rate, cells harbouring pGW155B attained larger population sizes than cells without it. I used this parameter to estimate the biomass yield (y) of both strains, a proxy for metabolic efficiency[21] defined as $y = K/glc$, where K is the population size in the equilibrium or *carrying capacity* and glc the supply of glucose. This metric suggests that R

bioRxiv preprint doi: https://doi.org/10.1101/810259; this version posted December 20, 2019. The copyright holder for this preprint (which was not certified by peer review) is the author/funder, who has granted bioRxiv a license to display the preprint in perpetuity. It is made available under aCC-BY-NC-ND 4.0 International license.

cells, despite their slower growth rate, were the most efficient of both types (Mann-Whitney U-test for differences in carrying capacity $p \approx 0.021$, Figures 1B and C). Another parameter that I found sensitive to pGW155B was the lag phase—the period where cells negotiate their transition into growth—and its duration was considerably longer for the construct R (Figure 1B, Mann-Whitney U-test $p < 0.001$). In other words, growth rate, yield and lag engaged in a trade-off that was previously unknown and that, in my experimental setting, is triggered by the acquisition of pGW155B.

I asked whether R can take advantage of this trade-off without using tetracycline, which enforces the maintenance of pGW155B, and avoid extinction[7]. I propagated a culture containing equal proportions of each construct in media without tetracycline (see methods), and transferred the mixture into a new microtitre plate with fresh media only when R-cells reached stationary phase (after $\sim$ 24h, see Figure 1A). I repeated this process for seven consecutive 24h seasons and, during this time, tracked the relative abundance of each type. As Figure 1E illustrates, R-cells remained a significant part of the mixture despite growing at slower rates. The trade-off can therefore be exploited by plasmid-harbouring microbes.

Rate-yield (RY) trade-off changes the interpretation of carriage costs. Now, lag, yield and growth rate are sensitive to plasmid carriage and engaged in a trade-off. But the one between growth rate and yield is particularly relevant for clinicians and evolutionary biologists, who measure drug sensitivity using different traits.

The former frequently measure changes in bacterial density across a range of antibiotic concentrations[22–25], whereas the latter measure changes in growth rate[6,8,26]. I therefore asked whether the above trade-off can influence the interpretation of antibiotic sensitivity tests, and exposed the strains S and R to a range of tetracycline concentrations to measure the minimum inhibitory concentration (MIC)—a metric of drug sensitivity commonly used in drug therapy design[27,28]. The plasmid borne by R increased its resistance to tetracycline by $\sim 3,000\%$ irrespectively of the trait I measured (Mann-Whitney U-test $p = 0.083$, ranksum $= 55$), but the MIC reported was, indeed, different for each trait (Figures 2A and S1A). Using growth rate data, the minimum inhibitory concentration for R was 8.343 ± 0.288 µg/mL of tetracycline (mean $\pm$ 95% confidence, Figure 2A), whereas using bacterial density data the MIC was 6.106 ± 0.272 µg/mL (Figure S1A). That is a $\sim 35\%$ difference in the estimation of the same parameter. I found a similar gap for the tetracycline-sensitive strain S.

Prior literature[7] showed that costly plasmids are purged from bacterial populations at an exponential rate very rapidly, so it is reasonable to assume that the construct S—without pGW155B—will outgrow R in sustained pairwise competitions. But given the RY trade-off, it is no longer trivial to estimate the costs and consequences of plasmid carriage: Growth rate and lag data suggests that pGW155B is, indeed, costly to maintain (Figures 1A and S1B) but culture density data suggests it is beneficial. This uncertainty can be specially problematic for the estimation of mutant selection windows.

The range of antimicrobial concentrations that select for drug-resistant mutants is known as the 'mutant selection window'[6,29]. Microbes that carry chromosomal mutations, or indeed

bioRxiv preprint doi: https://doi.org/10.1101/810259; this version posted December 20, 2019. The copyright holder for this preprint (which was not certified by peer review) is the author/funder, who has granted bioRxiv a license to display the preprint in perpetuity. It is made available under aCC-BY-NC-ND 4.0 International license.

plasmids that protect them against antimicrobials incur in resistance costs that reduce the cell's growth rate[6,7,24,30]. It is predicated that, given these costs, selection on resistance occurs only when the antimicrobial drug is supplied at sufficiently high concentrations to leverage the difference in growth rate between sensitive and resistant types—the 'minimal selective concentration' or MSC[6]—existing a range of drug concentrations that optimally select for resistant mutants[6,29]. As I demonstrate below, resistant cells that exploit the above trade-off can be selected below MSCs.

The MSC for the construct R laid at 0.052 ± 0.004 µg/mL of tetracycline (Figure 2A). To test whether microbes exploiting a trade-off between growth rate and yield are still selected consistently with the mutant selection window hypothesis, I exposed a mixed culture containing equal proportions of each construct to a range of tetracycline concentrations. As above, the mixed culture was propagated after 24h into a microtitre plate with fresh media and antibiotic, and repeated the transfers for seven consecutive 24h seasons. The MSC did not change substantially throughout the competition (Kruskal-Wallis H-test $p = 0.3406$, χ^2-statistic $= 6.7912$, Figure 2B), thus, it is reasonable to expect that R will be selected with higher tetracycline concentrations. The selection coefficient[31] shows there was, indeed, selection for the construct R (Figure 2C), however, the selection coefficient for R was positive below the MSC. In other words, the construct R—harbouring pGW155B—was selected at lower-than-expected tetracycline concentrations. Growth rate data was not informative of this selection process (Figure 2D), but it was with cell density data (Figure 2E) where the construct R is more abundant that S across all conditions.

Note the change in costs of pGW155B with respect to those in Figure 1B. First, in mixed culture conditions both constructs reached lower densities as glucose, the carbon source, is now shared between two types of microbe—as opposed to one in pure culture conditions. But, given the trade-off between growth rate and yield resulting from pGW155B carriage, R divides faster in mixed culture (Mann-Whitney U-test for growth rate in absence of tetracycline, pure *versus* mixed conditions, $p = 6.21 \times 10^{-4}$, ranksum $= 37$). And second, S is not fully inhibited in mixed culture conditions (Figure S2), resulting in detectable growth rates shows in Figure 2D. However its growth rate is higher than that measured in pure culture conditions at similar tetracycline concentrations. Thus, parameters such as the MSC measured in pure culture growth conditions, did not hold in competition.

R-mutants with additional copies of pGW155B selected below the MSC. The range of tetracycline concentrations that I used suppose less than 2% the minimum inhibitory concentration for the construct R, however, Figure 2D shows that its growth rate declined with increasing tetracycline concentrations during the first season. However, in the last season, its growth rate remained unchanged. Figure 3A illustrates the relative difference in growth rate between both seasons, showing an increase in growth rate for the construct R over time that correlates with tetracycline concentration (linear regression $p \approx 1.45 \times 10^{-4}$, F-statistic$= 16.7$, adjusted coefficient of determination $R^2 = 0.222$; slope parameter $1.876, p \approx 1.99 \times 10^{-4}$, t-statistic$= 3.9915$). Importantly, yield and lag duration declined with higher drug concentra-

bioRxiv preprint doi: https://doi.org/10.1101/810259; this version posted December 20, 2019. The copyright holder for this preprint (which was not certified by peer review) is the author/funder, who has granted bioRxiv a license to display the preprint in perpetuity. It is made available under aCC-BY-NC-ND 4.0 International license.

tions in the same period of time (Figures 3B and C), consistently with the above trade-off. Importantly, these changes were absent in the construct S with growth rate, yield, and lag not trading-off (Figure S3); so I asked whether the number of plasmids borne by R cells changed through time with different tetracycline concentrations. It did.

To quantify the relative abundance of pGW155B within R cells, I sampled the mixed cultures on days one and five, calculated the proportion of chromosomal DNA corresponding to the construct R, and used quantitative polymerase chain reaction (qPRC) to measure the number of plasmids borne per cell (see methods). The initial pool of cells from this strain, grown overnight and used to inoculate the cultures, contained 30.21 ± 6.72 copies of pGW155B per cell (mean $\pm$ 95% confidence, $n = 3$). Without tetracycline, this number did not change significantly after one and five days of competition against S (Mann-Whitney U-test $p = 0.1$, ranksum $= 15$, Figure 3D). But the relative abundance of pGW155B changed rapidly with increasing drug concentrations. Within 24h the gain in plasmids was 2-fold, increasing 6- to 10-fold after five days of competition depending on tetracycline concentration (Figures 3E and F).

To understand the relationship between plasmid copy number and drug concentration I fitted two mathematical models to qPCR data. First the linear model $p_c = p_0 + d\kappa$ and then the constant model $p_c = \kappa$, where κ denotes the slope or proportionality constant, p_0 the initial number of copies borne by each R cell and d the antibiotic supplied. The constant model, that assumes no change in the number of plasmids borne per cell, was extremely unlikely (relative likelihood $\approx 6.80 \times 10^{-42}$, Figure 3E). Instead the linear model suggests that plasmid copy number correlates with drug concentration, where the constant of proportionality $\kappa = 161.87 \pm 110.37$ plasmids per mL per microgram of drug per cell (t-statistic $= 2.8745$, $p = 0.0088$ and 95% confidence interval (51.5, 272.2)). Albeit significant, with an adjusted coefficient of determination (R^2) of 0.245, the linear model does not entirely capture the dynamics of qPCR data. A switch-like, non-linear model, say, the logistic model (see methods), explained better the variation in the number of pGW155B that I observed (adjusted R^2 of 0.477). After five days of exposure to tetracycline the constant κ increased from 161.87 ± 110.37 to 880.19 ± 705.71 plasmids per mL per microgram of drug per cell (Figure 3F, t-statistic $= 2.4446$, $p = 0.0229$, and 95% confidence interval (174.5, 1585.9)). The predictive power declined for the logistic model, albeit it was still better than that for the linear model (adjusted $R^2 = 0.394$ *versus* 0.261).

Plasmid gains through random segregation. Now the question is this: how did R cells gain additional copies of pGW155B? Note that *E. coli* cannot share the plasmid horizontally given pGW155B lacks the genes needed for horizontal gene transfer[16,32] (addgene vector database accession code 2853). So, I hypothesised the following: That random segregation, the mechanism underlying plasmids loss in the absence of selection[7], can also facilitate their accumulation in bacteria. Suppose a microbe that harbours a plasmid and neither the microbe's chromosome nor the plasmid can mutate. If this microbe bears n copies of the plasmid and it replicates alongside the host's chromosome, the only means to gain or lose plasmids would be through the imperfect segregation of plasmids during cell division: one daughter cell would carry $n + 1$ plasmids whereas the other is left with $n - 1$. This process is how pGW155B, I hypothesise,

bioRxiv preprint doi: https://doi.org/10.1101/810259; this version posted December 20, 2019. The copyright holder for this preprint (which was not certified by peer review) is the author/funder, who has granted bioRxiv a license to display the preprint in perpetuity. It is made available under aCC-BY-NC-ND 4.0 International license.

changed its relative abundance in *E. coli*.

The microbe's growth depends upon the active uptake of a carbon source, S, from the environment, and it is inhibited by an antibiotic A. Based on these assumptions, I developed a theoretical framework and used it to predict how the relative number of plasmids would change through time when the bacterium is exposed to different concentrations of an antibiotic (see methods). I implemented this hypothesis as a Markov process, where the segregation of plasmids during cell division events is stochastic and independent of previous events. Assuming that only one plasmid can be gained or lost during each event with probability σ, I defined the growth of a microbial population, B, as

$$\frac{dB}{dt} = \mathcal{M}(1-c)\cdot G(A,S)\cdot B, \tag{1a}$$

$$\frac{dA_i}{dt} = -d\cdot A_i + \phi\sum B\cdot(A_e - A_i), \tag{1b}$$

$$\frac{dA_e}{dt} = -d\cdot A_e - \phi\sum B\cdot(A_e - A_i), \tag{1c}$$

$$\frac{dS}{dt} = -U\cdot\sum B, \tag{1d}$$

where the uptake rate is given by

$$U(S) = \frac{u_{max}S}{k_m + S} \tag{2}$$

and the growth function by

$$G(A,S) = y\cdot U(S)\cdot \underbrace{\frac{1}{1+\kappa A^2}}_{\text{A-Inhibition}}. \tag{3}$$

Here the growth function $G(A,S)$ depends on the antibiotic A and carbon S supplied. The carbon uptake follows Michaelis-Menten kinetics, with the maximum uptake rate given by u_{max} and k_m is the associated half-saturation constant. The antibiotic A, however, diffuses from the environment (A_e) into the cells (A_i) with a rate ϕ. The affinity of A for its target is given by the constant κ and the Hill coefficient 2. Finally, the carbon captured by B cells is transformed into biomass with yield y. B cells can harbour a plasmid so the associated cost of carriage is given by c in equation 1d, which will vary depending upon the number of plasmids borne. Inherent to the model is the emergence of subpopulations carrying different number of plasmids, from 0 to $j-1$ copies. Due to computational constraints I imposed j maximum copies and assumed that, once the plasmid is lost, it cannot be recovered. The following transition probability matrix, $\mathcal{M}$, defines the relative abundance of each subpopulation

$$\mathcal{M} = \begin{pmatrix} 1 & \sigma & 0 & & \cdots & 0 \\ 0 & 1-2\sigma & \sigma & 0 & & \vdots \\ 0 & \sigma & 1-2\sigma & \sigma & \ddots & \\ & 0 & \sigma & 1-2\sigma & \ddots & 0 \\ \vdots & & \ddots & \ddots & \ddots & \sigma \\ 0 & \cdots & & 0 & 0 & 1-\sigma \end{pmatrix}.$$

bioRxiv preprint doi: https://doi.org/10.1101/810259; this version posted December 20, 2019. The copyright holder for this preprint (which was not certified by peer review) is the author/funder, who has granted bioRxiv a license to display the preprint in perpetuity. It is made available under aCC-BY-NC-ND 4.0 International license.

Figures 3G and H illustrate the qualitative change in population structure resulting from the exposure to the antibiotic A. When the microbe grows in the absence of drug, the subpopulation with fewer copies of the plasmid is more abundant whereas those containing more copies of it are rare. However, the distribution changes when the microbe is exposed to A. The optimal number of plasmids changes in the presence of drug, and so, with more antibiotic the most frequent subpopulation harbours more copies of the plasmid.

The experimental data set is consistent with this prediction (Figures 3I, J, and K). If the initial pool of *E. coli* cells contained 30.21 ± 6.72 copies of the plasmid, after 24h of antibiotic challenge cells containing more copies rapidly emerged. The resulting distribution followed a Nakagami distribution (corrected Akaike Information Criterion AICc = 198.14, Negative Log-Likelihood $NLogL = 96.79$. See Methods) with parameters for shape $\mu = 2.18$ and scale $\omega = 1.79 \times 10^3$ (95% confidence intervals are $\mu = (1.29, 3.71)$ and $\omega = (1367.1, 2348.9)$). The mean copies of plasmids borne per cell after this period were 39.95 ± 10.58 (mean $\pm$ 95% confidence). These parameters changed when I prolonged the antibiotic challenge. After 120h of exposure to tetracycline the mean copies per cell increased to 169.58 ± 90.14 and the resulting distribution now followed a skewed Birnbaum–Saunders distribution (AICc = 290.19, NLogL = 142.81 *versus* AICc = 293.66 and NLogL = 144.54 for the Nakagami distribution) with parameters for shape $\gamma = 0.73$ and scale $\beta = 133.52$ (95% confidence $\gamma = (97.07, 169.98)$ and $\beta = (0.52, 0.94)$). Thus, the antibiotic challenge increased the frequency of cells bearing more copies of pGW155B consistently with this theory (Figure 3G) where the imperfect segregation of plasmid during cell division is the underlying mechanism.

Discussion

Studies that look beyond the effect of plasmids on growth rate are extremely rare[12,13]. Growth rate is associated with 'fitness' in microbes[5,8,30] and, therefore, it is used to measure the costs of plasmid carriage[7,33,34]. My study suggests, however, that plasmids alter more than just growth rate. This expands the number of traits that selection can act upon, in principle, regardless of the genes borne by plasmids and the trade-off between growth rate and yield that I report, mediated by the acquisition of pGW155B, is an example of this. Now, this begs the question of whether growth rate is a reliable predictor of plasmid maintenance or, more generally, the outcome of pairwise competitions. In my study it was not, given the trade-off between growth rate and yield, and that I favoured yield over growth rate to maintain pGW155B in R-cells without using tetracycline. This shows that 'costs' of plasmid carriage, or indeed, antimicrobial resistance are relative. However, I do not wish to overstate my results. Plasmids are incredibly diverse in terms of size, genes, or transfer mechanism[32], so the trade-off may be absent in other types of plasmid. Nevertheless, this highlights that plasmids are not molecular parasites[5,35] necessarily and may provide their hosts with more benefits than previously thought.

The relativity of 'costs', and importantly the relativity of drug sensitivity, poses serious challenges to rationales, like the 'mutant selection window', that rely on plasmids or resistance costs. However, it also open new opportunities for drug therapy design. For example, if antibiotic

bioRxiv preprint doi: https://doi.org/10.1101/810259; this version posted December 20, 2019. The copyright holder for this preprint (which was not certified by peer review) is the author/funder, who has granted bioRxiv a license to display the preprint in perpetuity. It is made available under aCC-BY-NC-ND 4.0 International license.

sensitivity depends on the trait used to assess it: Which one should be used to determine inhibitory concentrations and selection windows? Pathogens have different growth dynamics, with some dividing at faster rates than others[36–38], so, it seems reasonable, drug sensitivity based on growth rate data could be more informative of the microbe's sensitivity than sensitivity based on cell density data. But the relativity of costs and sensitivity can also have its drawbacks. For example, some traits may report a minimal selective concentration whereas other may not. The mutant selection window hypothesis claims that drug concentrations below the minimal selective concentration do not select for resistance[6,8,26], however, antimicrobial-resistance genes (ARG) are increasingly detected in environments with residual drug concentrations[39]. The relationship between traits—here growth rate and yield—will determine whether such 'safety' net exists or not.

The changes in plasmid copy number that I found were unexpected, given the low tetracycline concentrations used and, particularly, the lack of horizontal gene transfer mechanisms. Plasmid DNA can be substantially higher than chromosomal DNA in bacteria[40], and its relative abundance can change within the body during infections[41]. It is therefore surprising that international AMR surveillance programmes[42] track only whether pathogens harbour plasmids, overlooking their relative abundance within the cell. This has practical implications. For example, the curation of plasmids from bacteria *in vivo* is gaining momentum as an alternative to treat drug-resistant infections[43–46]. But the technique is still inefficient. It should be self-evident that pathogens carrying fewer plasmids will be easier to treat than those bearing more copies of them, but the variations in the number of plasmids borne are often overlooked. Equally, microbes hosting more plasmids with antimicrobial-resistance genes should be less sensitive to antibiotics than those harbouring fewer plasmids—despite harbouring *exactly* the same plasmid. Reporting this information will be an asset in our fight against antimicrobial-resistant microbes.

Methods

Media and Strains. I used the strains of *Escherichia coli* GB(c) and Wyl[47] (a gift from Remy Chait and Roy Kishony), and M9 minimal media supplemented with 0.4% glucose and 0.1% casamino acids. I made tetracycline stock solutions from powder stock (Duchefa #0150.0025) at 5mg/mL in deionised water. Subsequent dilutions were made from this stock and kept at 4°C.

Batch transfer protocol. I inoculated a 96-well microtitre plate containing 150µg/mL of media supplemented with tetracycline with a mixture of two overnight cultures, one of *E. coli* GB(c) and another of *E. coli* Wyl (Figure S4). The overnight culture for GB(c) was supplemented with 100ng/mL of tetracycline to preserve the plasmid pGW155B carrying *tet(36)*[47], centrifuged and removed prior adding to the microtitre plate. I incubated the plate at 30°C in a commercial spectrophotometer and measured the optical density of each well at 600nm (OD_{600}), yellow florescence for the S strain (YFP excitation at 505nm, emission at 540nm), and cyan fluorescence for the R strain (CFP at 430nm/480nm) every 20min for 24h (a.k.a. *season*). After each season I transferred 1.5µL of each well, using a 96-well pin replicator, into

bioRxiv preprint doi: https://doi.org/10.1101/810259; this version posted December 20, 2019. The copyright holder for this preprint (which was not certified by peer review) is the author/funder, who has granted bioRxiv a license to display the preprint in perpetuity. It is made available under aCC-BY-NC-ND 4.0 International license.

a new microtitre plate containing fresh growth medium and tetracycline.

Growth parameter estimation. Fluorescence protein genes were constitutively expressed with an approximately constant fluorescence to optical density ratio (Figure S5). This enabled me to use fluorescence as a proxy for culture density in mixed culture conditions. I normalised fluorescence readings with respect to optical density using the ratio OD to fluorescence in pure culture conditions as a reference.

I imported the resulting OD time series data set (Figures S6 and S7) into `MATLAB R2014b` to subtract background and calculate growth rate *per capita* (fitness, f) using the following algorithm. First, I fitted three mathematical models to data: 1) linear model $g(t) = b + f \cdot t$, 2) exponential model $g(t) = b + C \cdot \exp(f \cdot t)$ and 3) logistic model $g(t) = b + K/(1 + C \cdot \exp(-f \cdot t))$. The terms $g(t)$ denote culture growth through time (in OD, YFP, or CFP units), b the inoculum size used to subtract the background, C is a parameter and K the maximal population size attained. I used the fitness reported by the model with the lowest corrected Akaike Information Criterion (AICc). To estimate the biomass yield I divided OD data in stationary phase by the glucose supplied[21]. I also used the highest density at any given time and the density reported by the data fit, both divided by glucose supply, as alternative metrics for biomass yield.

Finally, I calculated the selection coefficient for the plasmid-harbouring strain using the regression model[31] $s = ln[R(t)/R(0)] \cdot t^{-1}$, where $R(0)$ is the initial ratio of resistant to susceptible (1:1) and $R(t)$ the ratio at time t.

Drug sensitivity parameter estimation. I defined the minimum inhibitory concentration (MIC) for each trait as the tetracycline required to reduce the trait of the bacterium by a factor of 99%, compared to the tetracycline-free control. The MICs were 0.364 ± 0.012 (mean $\pm$ 95% confidence), and 0.351 ± 0.013 of tetracycline for the strain S using culture density and growth rate, respectively. For the strain R they were 11.121 ± 1.734, and 9.103 ± 0.379 µg/mL. Given the suppression of S in competition (Figure S2), I failed to detect its MICs in these conditions. I therefore relaxed the degree of inhibition from 99% to 90% (IC_{90}) to allow the estimation of drug sensitivity parameters in competition.

DNA material extraction. For each concentration, I sampled three representative 150µg/mL cultures that I divided into two groups for chromosome and plasmid DNA extraction. I ThermoScientific GeneJet DNA (#K0729) and GeneJet Plasmid (#K0502) extraction kits to extract chromosome and plasmid DNA from the samples, respectively, and used Qubit to quantify the yields. Both extracts were diluted accordingly in extraction buffer to normalise DNA across samples.

Quantitative PCR and plasmid copy number estimation. I used `primer3` to design two pairs of primers with melting temperature (T_m) of 60^oC and non-overlapping probes with T_m of 70^oC. The amplicon ranges between 100 to 141bp depending on the locus (Table S1). Two reaction mixes were prepared using the kit 'Luminaris Color Probe Low ROX' (ThermoScientific

bioRxiv preprint doi: https://doi.org/10.1101/810259; this version posted December 20, 2019. The copyright holder for this preprint (which was not certified by peer review) is the author/funder, who has granted bioRxiv a license to display the preprint in perpetuity. It is made available under aCC-BY-NC-ND 4.0 International license.

#K0342), adding 0.3µM of each primer and 0.2µM of the probe as per manufacturer specifications. Following a calibration curve for each reaction (Figure S8) I added 0.01ng of chromosomal or plasmid DNA material to each of the reaction mixes.

To estimate the relative copies of pGW155B per R cell, I calculated the corresponding proportion of chromosomal DNA corresponding to the R-type from data in Figure 2D and used the formula[7]

$$cn = \frac{(1+E_c)^{Ctc}}{(1+E_p)^{Ctp}} \times \frac{S_c}{S_p},$$

where cn is the number of plasmid copies per chromosome, S_c and S_p are the size of the chromosome and pGW155B amplicon in bp, E_c and E_p the efficiency of the qPCR taken from data in Figure S8, and Ctc and Ctp are the cycles at which I first detected product amplification (C_t).

Distribution fit to data. To find the distribution that best fits qPCR data, I tried all distributions available in `MATLAB 2014a` using the built-in routine `fitdist`. I then used the negative log-likelihood (NLogL) function and corrected Akaike Information Criterion (AICc) as metrics for the goodness of fit, and sorted the distributions accordingly. Finally, I considered the best fit that distribution with the lowest NLogL and AICc.

bioRxiv preprint doi: https://doi.org/10.1101/810259; this version posted December 20, 2019. The copyright holder for this preprint (which was not certified by peer review) is the author/funder, who has granted bioRxiv a license to display the preprint in perpetuity. It is made available under aCC-BY-NC-ND 4.0 International license.

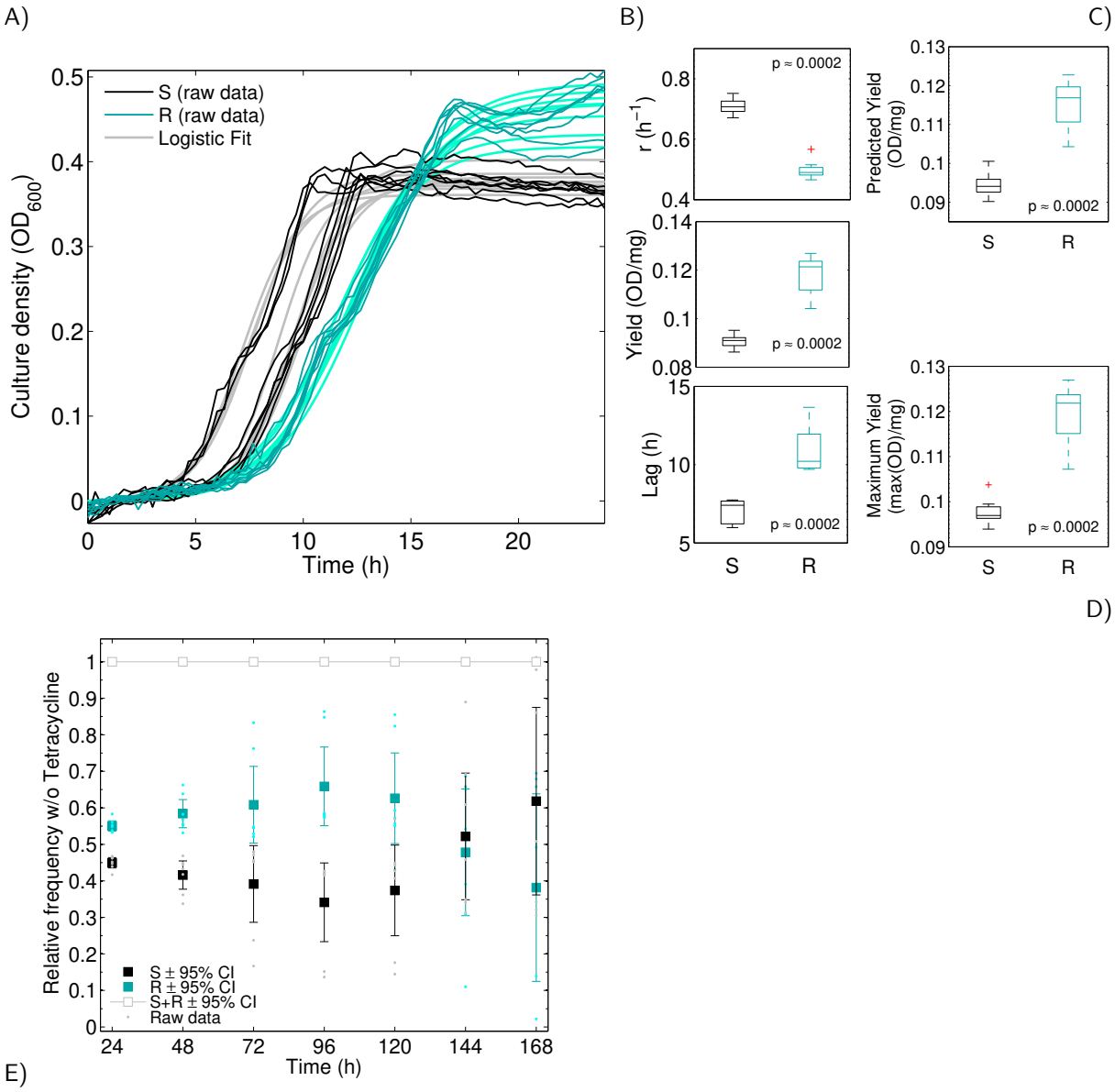

FIGURE 1. Rate-yield-lag (RYL) trade-off in construct harbouring pGW155B. A) Overlapped growth curves of strains S (black) and R (cyan) in the absence of tetracycline. I estimated the growth rate (r) *per capita*, population size in the equilibrium (K), biomass yield (see main text), and lag from logistic models fitted to data (see Methods) shown in grey and light cyan, respectively. **B)** Box plots for each trait showing the median (centre of the box), 25th and 75th percentile of the data set. The whiskers extend to the most extreme data points that are not outliers, and these are individually represented. The p value shown on top of each box plot refers to a Mann-Whitney U-test that I used to test differences in the parameters between both strains. **C-D)** Alternative metrics for biomass yield (see methods) using culture density reported by the data fit (C) and maximal culture density at any given time (D). The p values correspond to Mann-Whitney U-tests. **E)** Relative frequency (mean ± 95% CI) of each construct during a 7-day long pairwise competition in the absence of tetracycline.

bioRxiv preprint doi: https://doi.org/10.1101/810259; this version posted December 20, 2019. The copyright holder for this preprint (which was not certified by peer review) is the author/funder, who has granted bioRxiv a license to display the preprint in perpetuity. It is made available under aCC-BY-NC-ND 4.0 International license.

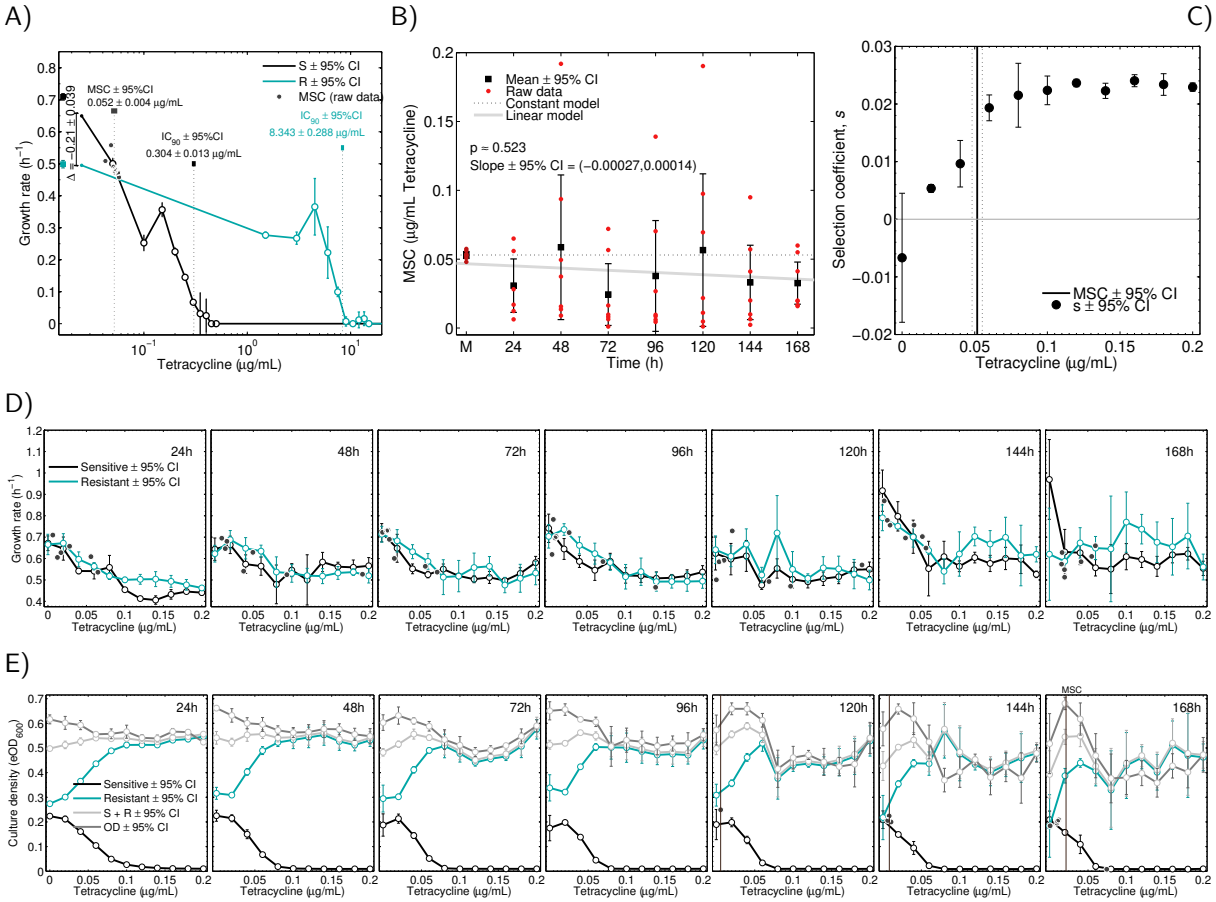

FIGURE 2. Construct R selected below the minimal selective concentration. A) Dose-response profile for each strain showing the change in growth rate with increasing tetracycline concentrations. I measured the costs of carrying pGW155B using growth rate from relative fluorescence growth data, with a decrease of 0.21 ± 0.039 h^{-1} for R (mean ± 95% confidence, $n = 8$). The profiles of both strains crossed-over with 0.052 ± 0.004 µg/mL of tetracycline, defining the *minimal selective concentration*. **B)** Change in MSC over time with respect that measured in monoculture (M). Mean and 95% confidence interval are shown as black errorbars and the raw data as red dots. I fitted this data set to a constant (dotted line) and linear (light grey) models, the p value and slope shown correspond to the linear model. **C)** Selection coefficient for the resistant strain, s, at different tetracycline concentrations. I also represented the MSC in B) and its 95% confidence interval as a reference. **D)** Change in *per capita* growth rate during the 7-day pairwise competition showing both sensitive (S, black) and resistant (R, cyan) constructs of *Escherichia coli*. In each subplot I present the mean growth rate ± 95% confidence ($n = 8$) across all tetracycline concentration corresponding to seven consecutive 24h seasons. The crossing point for each replicate—minimal selective concentration or MSC—is shown as small, black circles. **E)** Same as D), but I show change in cell density in optical density units derived from normalised fluorescence data (see methods). In light grey I show the optical density of the mixed culture estimated from normalised fluorescence data, and in dark grey the optical density measured at 600nm.

bioRxiv preprint doi: https://doi.org/10.1101/810259; this version posted December 20, 2019. The copyright holder for this preprint (which was not certified by peer review) is the author/funder, who has granted bioRxiv a license to display the preprint in perpetuity. It is made available under aCC-BY-NC-ND 4.0 International license.

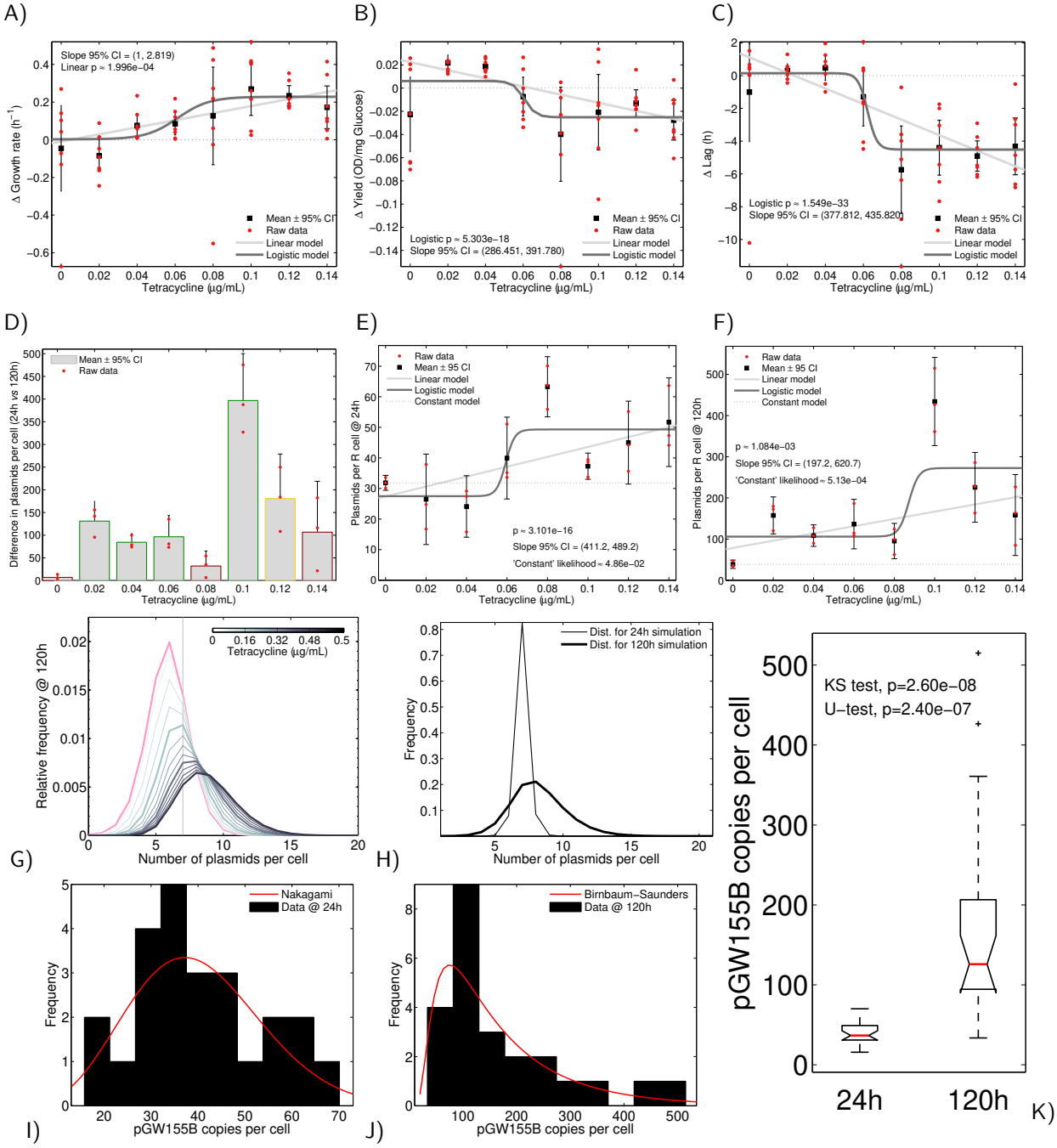

bioRxiv preprint doi: https://doi.org/10.1101/810259; this version posted December 20, 2019. The copyright holder for this preprint (which was not certified by peer review) is the author/funder, who has granted bioRxiv a license to display the preprint in perpetuity. It is made available under aCC-BY-NC-ND 4.0 International license.

Figure 3. Tetracycline-induced variation in pGW155B copy number results phenotypic changes compatible with the RYL trade-off. A-C) Change in growth rate (A), biomass yield (B), and lag (C) after 168h exposure to different tetracycline concentrations. I show mean and 95% confidence interval as black error bars and raw data in red dots. The dotted black line represents a constant model (a.k.a. no change), light grey line represents a linear model, and dark grey a logistic model. The statistics shown in A-C are those for the model with the lowest corrected Akaike Information Criterion (AICc). **D)** Variation in pGW155B copy number after five days (120h) of exposure to tetracycline. Bars denote the mean and the errorbar 95% confidence of the mean; those with a green edge have a significant increase in copy number ($p < 0.05$) according to Welch's t-test, red if it was not ($p > 0.05$), and yellow if the test was inconclusive ($p \approx 0.05$). Raw difference in qPCR data is shown as red dots. **E-F)** Copies of pGW155B borne by R cells exposed to different tetracycline concentrations after 24h (E) and 120h (F). I show the mean and 95% confidence interval of qPCR data as black errorbars, and raw qPCR data as red dots. The black dotted line represents the prediction from the constant model, in light grey that for the linear model, and in dark grey the prediction for the logistic model. Statistical significance (p) for the slope parameter and confidence interval is shown for the model with lowest corrected Akaike Information Criterion, which was the logistic in both data sets: 190.153 *versus* 184.106 for 24h data (linear *versus* logistic), and 305.586 *versus* 290.435 for 120h data. The likelihood function deemed the constant model unlikely (probability of 0.0486 for 24h data, 0.0005 for 120h data), so I did not consider its AICc. **G)** Theoretical distributions of plasmid copy number as a function of antibiotic concentration. The thin, vertical line illustrates the initial distribution of plasmids—analog to the inoculum in the experimental setup. The distribution of plasmids for each drug concentration is shown in different colours from light green (low drug) to black (high drug), with thicker lines denoting higher drug concentrations. The distribution in the absence of antibiotic is shown in pink. **H)** Pooled frequency of plasmids after 24h and 120h of exposure to the drug using simulated data. **I-J)** Distribution of pGW155B copies in R-cells after 24h (I) and 120h (J) of exposure to tetracycline based on qPCR data. In red I represent the continuous distributions that best fit the data (red lines, see methods): 'Nakagami' for the 24h dataset and 'Birnbaum–Saunders' for the 120h dataset. **K)** Two-sample Kolmogorov-Smirnov (KS) and Mann–Whitney U-tests to test whether both datasets come from different distributions. The box plot shows the median (red), 75th and 25th percentile of the data set, and the whiskers extend to the most extreme data points not considered outliers. The outliers are plotted individually.

bioRxiv preprint doi: https://doi.org/10.1101/810259; this version posted December 20, 2019. The copyright holder for this preprint (which was not certified by peer review) is the author/funder, who has granted bioRxiv a license to display the preprint in perpetuity. It is made available under aCC-BY-NC-ND 4.0 International license.

References

1. Slater, F. R., Bailey, M. J., Tett, A. J. & Turner, S. L. Progress towards understanding the fate of plasmids in bacterial communities. *FEMS Microbiol. Ecol.* **66,** 3–13 (2008).
2. Harrison, E. & Brockhurst, M. A. Plasmid-mediated horizontal gene transfer is a coevolutionary process. *Trends Microbiol.* **20,** 262–267 (2012).
3. Esser, K., Kück, U., *et al. Plasmids of Eukaryotes: Fundamentals and Applications* ISBN: 9783642825859 (Springer Berlin Heidelberg, 2012).
4. Starikova, I., Sørum, V., *et al.* Fitness costs of various mobile genetic elements in Enterococcus faecium and Enterococcus faecalis. *J. Antimicrob. Chemother.* **68,** 2755–2765 (2013).
5. Bergstrom, C. T., Lipsitch, M. & Levin, B. R. Natural selection, infectious transfer and the existence conditions for bacterial plasmids. *Genetics* **155,** 1505–1519 (2000).
6. Gullberg, E., Cao, S., *et al.* Selection of resistant bacteria at very low antibiotic concentrations. *PLoS Pathog.* **7,** e1002158 (July 2011).
7. Millán, A. S., Peña-Miller, R., *et al.* Positive selection and compensatory adaptation interact to stabilize non-transmissible plasmids. *Nat. Commun.* **5** (2014).
8. Day, T., Huijben, S. & Read, A. F. Is selection relevant in the evolutionary emergence of drug resistance? *Trends Microbiol.* **23,** 126–133 (2015).
9. Sherratt, D. The Maintenance and Propagation of Plasmid Genes in Bacterial Populations The Sixth Fleming Lecture. *Microbiology* **128,** 655–661 (1982).
10. Byrd, J. J. & Colwell, R. R. Long-term survival and plasmid maintenance of Escherichia coli in marine microcosms. *FEMS Microbiol. Ecol.* **12,** 9–14 (1993).
11. Heuer, H, Krögerrecklenfort, E, *et al.* Gentamicin resistance genes in environmental bacteria: prevalence and transfer. *FEMS Microbiol. Ecol.* **42,** 289–302 (2002).
12. Rhee, J. I., Ricci, J. C. D., Bode, J. & Schügerl, K. Metabolic enhancement due to plasmid maintenance. *Biotechnol. Lett.* **16,** 881–884 (1994).
13. Diaz Ricci, J. C. & Hernández, M. E. Plasmid effects on Escherichia coli metabolism. *Crit. Rev. Biotechnol.* **20,** 79–108 (2000).
14. Gonçalves, G. A., Bower, D. M., Prazeres, D. M., Monteiro, G. A. & Prather, K. L. Rational engineering of Escherichia coli strains for plasmid biopharmaceutical manufacturing. *Biotechnol. J.* **7,** 251–261 (2012).
15. Baltrus, D. A. Exploring the costs of horizontal gene transfer. *Trends Ecol. Evol.* **28,** 489–495 (2013).
16. Chait, R., Shrestha, S., Shah, A. K., Michel, J.-B. & Kishony, R. A Differential Drug Screen for Compounds That Select Against Antibiotic Resistance. *PLoS One* **5,** e15179 (2010).

bioRxiv preprint doi: https://doi.org/10.1101/810259; this version posted December 20, 2019. The copyright holder for this preprint (which was not certified by peer review) is the author/funder, who has granted bioRxiv a license to display the preprint in perpetuity. It is made available under aCC-BY-NC-ND 4.0 International license.

17. Pfeiffer, T., Schuster, S. & Bonhoeffer, S. Cooperation and competition in the evolution of ATP-producing pathways. *Science* **292,** 504–507 (2001).

18. Novak, M., Pfeiffer, T., Lenski, R. E., Uwe Sauer & Bonhoeffer, S. Experimental Tests for an Evolutionary Trade-Off between Growth Rate and Yield in E. coli. *Am. Nat.* **168,** pp. 242–251. ISSN: 00030147 (2006).

19. Cheng, C., O'Brien, E. J., *et al.* Laboratory evolution reveals a two-dimensional rate-yield tradeoff in microbial metabolism. *PLoS Comput. Biol.* **15,** 1–17 (2019).

20. Scott, M., Klumpp, S., Mateescu, E. M. & Hwa, T. Emergence of robust growth laws from optimal regulation of ribosome synthesis. *Mol. Syst. Biol.* **10,** 747 (2014).

21. Reding-Roman, C., Hewlett, M., *et al.* The unconstrained evolution of fast and efficient antibiotic-resistant bacterial genomes. *Nat. Ecol. Evol.* **1,** 0050 (2017).

22. Andrews, J. M. Determination of minimum inhibitory concentrations. *J. Antimicrob. Chemother.* **48,** 5–16 (2001).

23. Drlica, K. & Zhao, X. Mutant selection window hypothesis updated. *Clin. Infect. Dis.* **44,** 681–8 (Mar. 2007).

24. Andersson, D. I. & Hughes, D. Antibiotic resistance and its cost: is it possible to reverse resistance? *Nat. Revs. Microbiol.* **8,** 260–271 (2010).

25. Choi, J., Yoo, J., *et al.* A rapid antimicrobial susceptibility test based on single-cell morphological analysis. *Sci. Transl. Med.* **6,** 267ra174 (2014).

26. Rosenbloom, D. I., Hill, A. L., Rabi, S. A., Siliciano, R. F. & Nowak, M. A. Antiretroviral dynamics determines HIV evolution and predicts therapy outcome. *Nat. Med.* **18,** 1378–1385 (2012).

27. Finberg, R. W. & Guharoy, R. in *Clinical Use of Anti-infective Agents* 5–14 (Springer, 2012).

28. Ajmal, S., Saleh, O. A. & Beam, E. Development of high-grade daptomycin resistance in a patient being treated for Corynebacterium striatum infection. *Antimicrob. Agents. Chemother.* **61** (2017).

29. Baquero, F. & Negri, M.-C. Challenges: Selective compartments for resistant microorganisms in antibiotic gradients. *Bioessays* **19,** 731–736 (1997).

30. Andersson, D. I. & Levin, B. R. The biological cost of antibiotic resistance. *Curr. Opin. Microbiol.* **2,** 489–493 (1999).

31. Dykhuizen, D. E. Experimental Studies of Natural Selection in Bacteria. *Annu. Rev. Ecol. Syst.* **21,** 373–398 (1990).

32. Smillie, C., Garcillán-Barcia, M. P., Francia, M. V., Rocha, E. P. & de la Cruz, F. Mobility of plasmids. *Microbiol. Mol. Biol. Rev.* **74,** 434–452 (2010).

bioRxiv preprint doi: https://doi.org/10.1101/810259; this version posted December 20, 2019. The copyright holder for this preprint (which was not certified by peer review) is the author/funder, who has granted bioRxiv a license to display the preprint in perpetuity. It is made available under aCC-BY-NC-ND 4.0 International license.

33. MacLean, R. C., Hall, A. R., Perron, G. G. & Buckling, A. The population genetics of antibiotic resistance: integrating molecular mechanisms and treatment contexts. *Nat. Rev. Genet.* **11,** 405 (2010).

34. Lopatkin, A. J., Meredith, H. R., *et al.* Persistence and reversal of plasmid-mediated antibiotic resistance. *Nat. Commun.* **8,** 1689 (2017).

35. Svara, F. & Rankin, D. J. The evolution of plasmid-carried antibiotic resistance. *BMC Evol. Biol.* **11,** 130 (2011).

36. Korem, T., Zeevi, D., *et al.* Growth dynamics of gut microbiota in health and disease inferred from single metagenomic samples. *Science* **349,** 1101–1106. ISSN: 0036-8075 (2015).

37. Leggett, H. C., Cornwallis, C. K., Buckling, A. & West, S. A. Growth rate, transmission mode and virulence in human pathogens. *Philos. Trans. R. Soc. Lond., B, Biol. Sci.* **372,** 20160094 (2017).

38. Gallagher, T., Phan, J. & Whiteson, K. Getting Our Fingers on the Pulse of Slow-Growing Bacteria in Hard-To-Reach Places. *J. Bacteriol.* **200** (ed DiRita, V. J.) ISSN: 0021-9193 (2018).

39. Pikkemaat, M., Yassin, H, Fels-Klerkx, H. & Berendsen, B. *Antibiotic residues and resistance in the environment* tech. rep. (RIKILT Wageningen UR, 2016).

40. Zhong, C., Peng, D., *et al.* Determination of plasmid copy number reveals the total plasmid DNA amount is greater than the chromosomal DNA amount in Bacillus thuringiensis YBT-1520. *PLoS One* **6,** e16025 (2011).

41. Wang, H., Avican, K., *et al.* Increased plasmid copy number is essential for Yersinia T3SS function and virulence. *Science* **353,** 492–495 (2016).

42. *European Centre for Disease Prevention and Control. EU protocol for harmonised monitoring of antimicrobial resistance in human Salmonella and Campylobacter isolates* tech. rep. (2016).

43. Baquero, F., Coque, T. M. & de la Cruz, F. Eco-Evo drugs and strategies: the need for novel tools to fight antibiotic resistance. *Antimicrob. Agents. Chemother.,* AAC–00013 (2011).

44. Bikard, D., Euler, C. W., *et al.* Exploiting CRISPR-Cas nucleases to produce sequence-specific antimicrobials. *Nat. Biotech.* **32,** 1146 (2014).

45. Kamruzzaman, M., Shoma, S., Thomas, C. M., Partridge, S. R. & Iredell, J. R. Plasmid interference for curing antibiotic resistance plasmids in vivo. *PloS One* **12,** e0172913 (2017).

46. Buckner, M. M., Ciusa, M. L. & Piddock, L. J. Strategies to combat antimicrobial resistance: anti-plasmid and plasmid curing. *FEMS Microbiol. Rev.* **42,** 781–804 (2018).

47. Chait, R., Craney, A & Kishony, R. Antibiotic interactions that select against resistance. *Nature* **446,** 668–671 (2007).

bioRxiv preprint doi: https://doi.org/10.1101/810259; this version posted December 20, 2019. The copyright holder for this preprint (which was not certified by peer review) is the author/funder, who has granted bioRxiv a license to display the preprint in perpetuity. It is made available under aCC-BY-NC-ND 4.0 International license.

Acknowledgements: I thank R. Beardmore for in-depth comments on the manuscript; R. Chait and members of the Beardmore and Gudelj laboratories for comments. **Competing interests:** The author declares no competing interests.

bioRxiv preprint doi: https://doi.org/10.1101/810259; this version posted December 20, 2019. The copyright holder for this preprint (which was not certified by peer review) is the author/funder, who has granted bioRxiv a license to display the preprint in perpetuity. It is made available under aCC-BY-NC-ND 4.0 International license.

Supplementary Tables

Table S1. Primers and probes designed using `Primer3`. Amplicon ranging from 100 to 141bp. T_m indicates the estimated melting temperature.

Target gen	Sequence ($5' \rightarrow 3'$)	T_m (^oC)	Feature
tatB	CGATGAAGCGTTCCTACGTT	60.27	Forward
	TCATGCGCAGCTTCATTATC	59.94	Reverse
	AAGGCGAGCGATGAAGCGCA	70.70	Probe
tet(36)	ATTGGGCATCTATTGGCTTG	59.22	Forward
	CCGATTCACAGGCTTTCTTG	60.76	Reverse
	AGCCTTTGCCAATTGGGGCG	70.37	Probe

Supplementary Figures

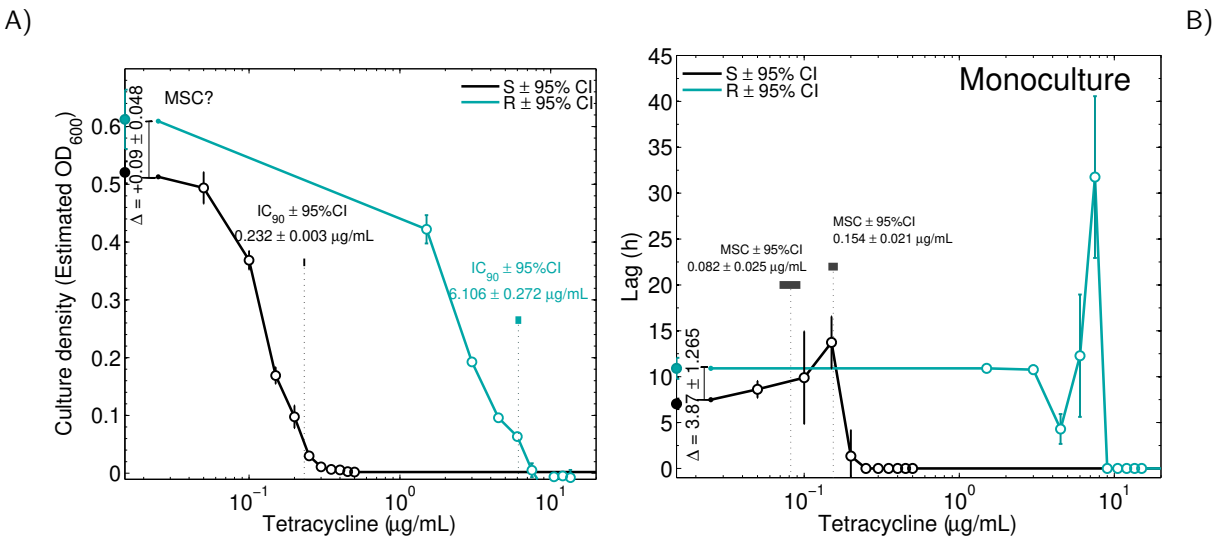

Figure S1. Dose-response profile for tetracycline using culture density and lag data. Dose-response profiles for each strain showing the change in culture density (A) and lag (B) with increasing tetracycline concentrations. The difference in R growth with respect to S was positive in antibiotic-free conditions (mean ± 95% confidence). Consequently, I could not detect any tetracycline concentration at which the profiles crossed over—*minimal selective concentration*—and establish the selection window for S. I estimated culture density from fluorescence data normalised with respect to optical density data (see methods). In lag data, the difference between both types without tetracycline was negative and, thus, I could detect two MSCs at 0,082 ± 0.025 and .0.154 ± 0.021 µg/mL of tetracycline.

bioRxiv preprint doi: https://doi.org/10.1101/810259; this version posted December 20, 2019. The copyright holder for this preprint (which was not certified by peer review) is the author/funder, who has granted bioRxiv a license to display the preprint in perpetuity. It is made available under aCC-BY-NC-ND 4.0 International license.

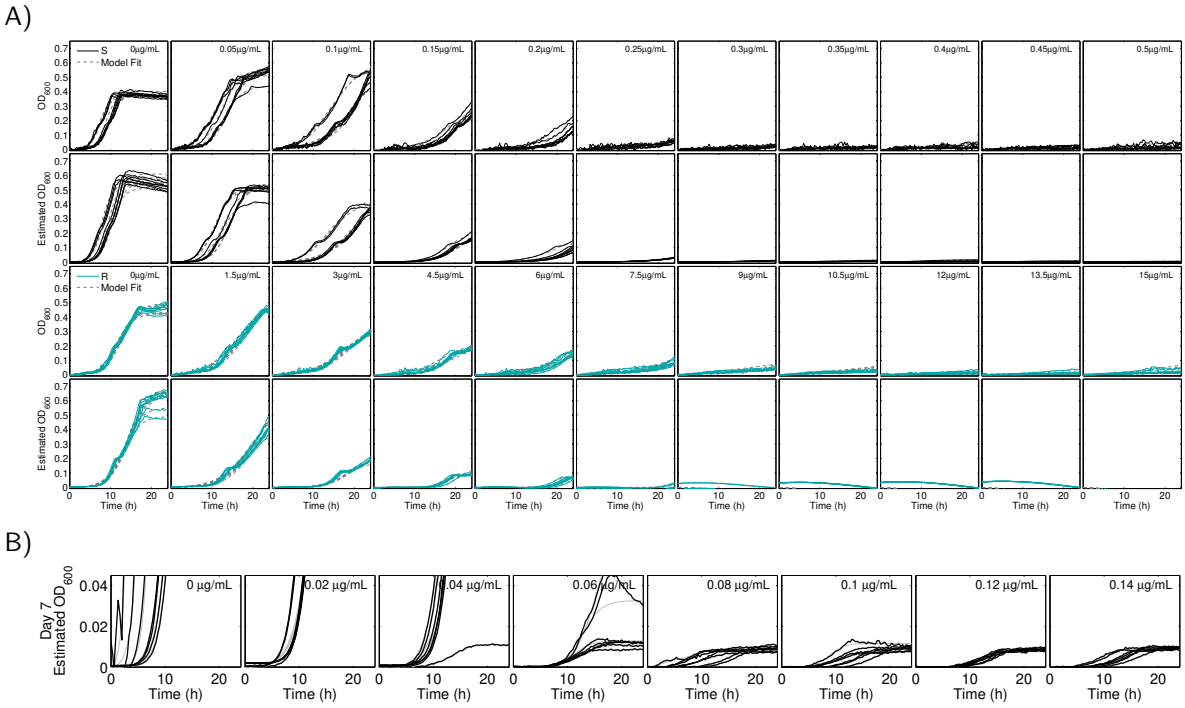

Figure S2. Sensitive type not fully outcompeted during the competition. A) Raw data for the construct S (black) and R (cyan) growing in M9 media supplemented with increasing tetracycline concentrations (different columns show different conditions). First and third rows show optical density data measured at 600nm, whereas second and fourth rows show density data estimated from relative fluorescence. **B)** Augmented detail of the evolved dose-response profiles of the tetracycline sensitive type S after seven days of exposure to tetracycline. Density data measured every 20min for seven 24h seasons (black) with the best fit to data (see main text) used to calculate growth parameters shown in grey. Each column represents the data set for one 24h season and each row the data set for one tetracycline concentration.

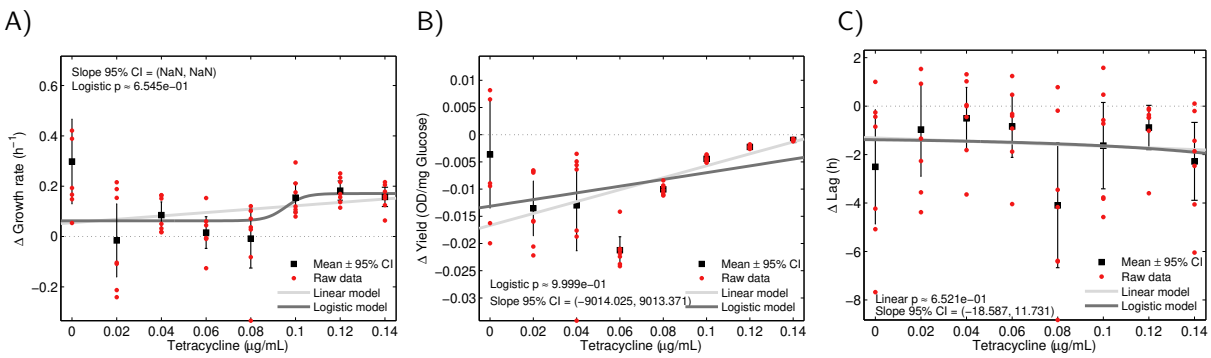

Figure S3. No rate-yield-lag (RYL) trade-off observed for the construct S. Variation in growth rate (A), biomass yield (B), and lag (C) after 168h exposure to different tetracycline concentrations. I show mean and 95% confidence interval as black error bars and raw data in red dots. The dotted black line represents a constant model (a.k.a. no change), light grey line represents a linear model, and dark grey a logistic model. The statistics shown in A-C are those for the model with the lowest corrected Akaike Information Criterion (AICc).

bioRxiv preprint doi: https://doi.org/10.1101/810259; this version posted December 20, 2019. The copyright holder for this preprint (which was not certified by peer review) is the author/funder, who has granted bioRxiv a license to display the preprint in perpetuity. It is made available under aCC-BY-NC-ND 4.0 International license.

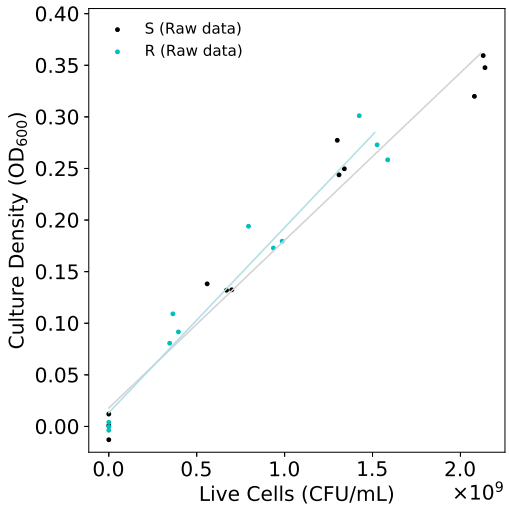

FIGURE S4. Calibration curve to translate optical density data to number of *Escherichia coli* cells. I fitted the linear model $a = bx + c$ to optical density and colony counting data (dots) to calculate the number of optical density units (OD_{600}) per cell. a denotes the optical density readings measured at 600nm, c the crossing point with the $y-$axis when $x = 0$, and b the conversion factor between optical density and number of cells (x). I interpolating optical density readings to calculate the number of cells within a culture as $x = (a - c)/b$. For the strain S, $b = 1.62 \times 10^{-10}\ OD \cdot mL \cdot CFU^{-1}$ and $c = 1.78 \times 10^{-2}\ OD$, whereas for R $b = 1.79 \times 10^{-10}\ OD \cdot mL \cdot CFU^{-1}$ and $c = 1.33 \times 10^{-2}\ OD$.

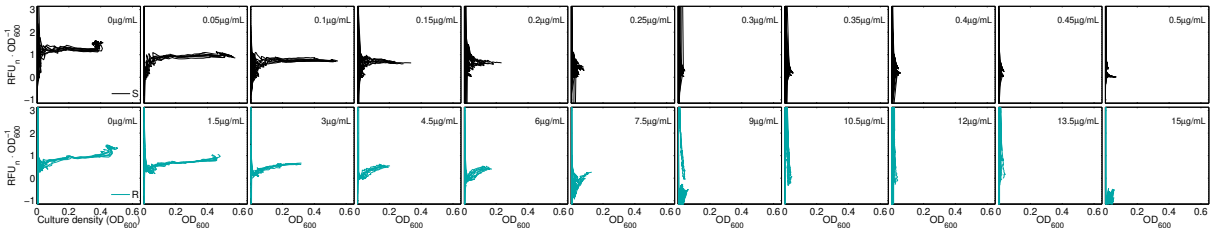

FIGURE S5. Changes in relative fluorescence over time in both R and S strains. Raw change in florescence, per optical density units, measured every 20min for 24h for the S- (black) and R-type. Each column represents the data set for each tetracycline concentration used.

bioRxiv preprint doi: https://doi.org/10.1101/810259; this version posted December 20, 2019. The copyright holder for this preprint (which was not certified by peer review) is the author/funder, who has granted bioRxiv a license to display the preprint in perpetuity. It is made available under aCC-BY-NC-ND 4.0 International license.

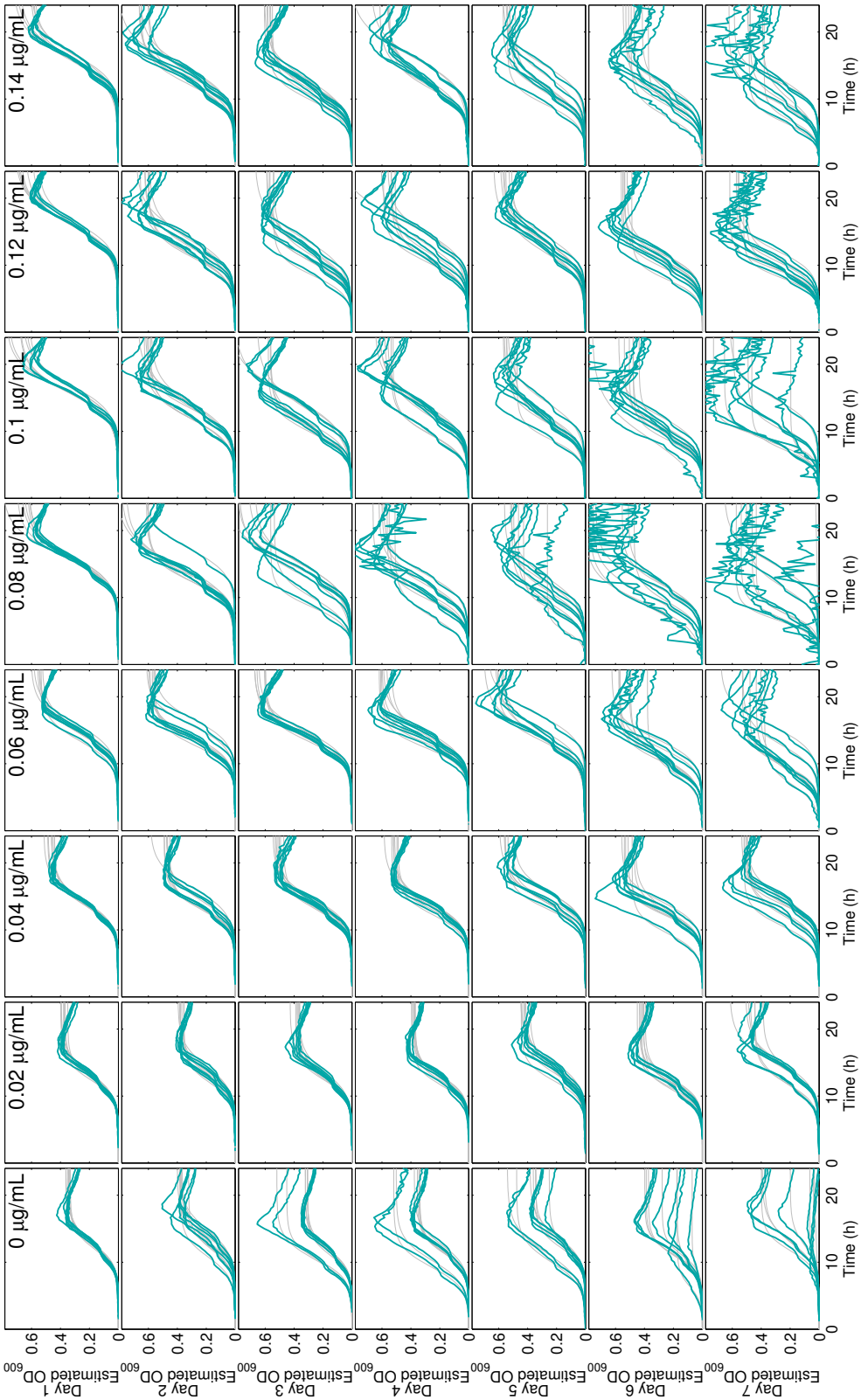

Figure S6. Raw data and model fit for resistant R strain. Raw optical Density data for GB(c) measured every 20min for seven 24h seasons (blue). The best fit to data (see methods in main text) used to calculate bacterial fitness is shown in grey. Each column represents the data set for one 24h season and each row the data set for one tetracycline concentration.

bioRxiv preprint doi: https://doi.org/10.1101/810259; this version posted December 20, 2019. The copyright holder for this preprint (which was not certified by peer review) is the author/funder, who has granted bioRxiv a license to display the preprint in perpetuity. It is made available under aCC-BY-NC-ND 4.0 International license.

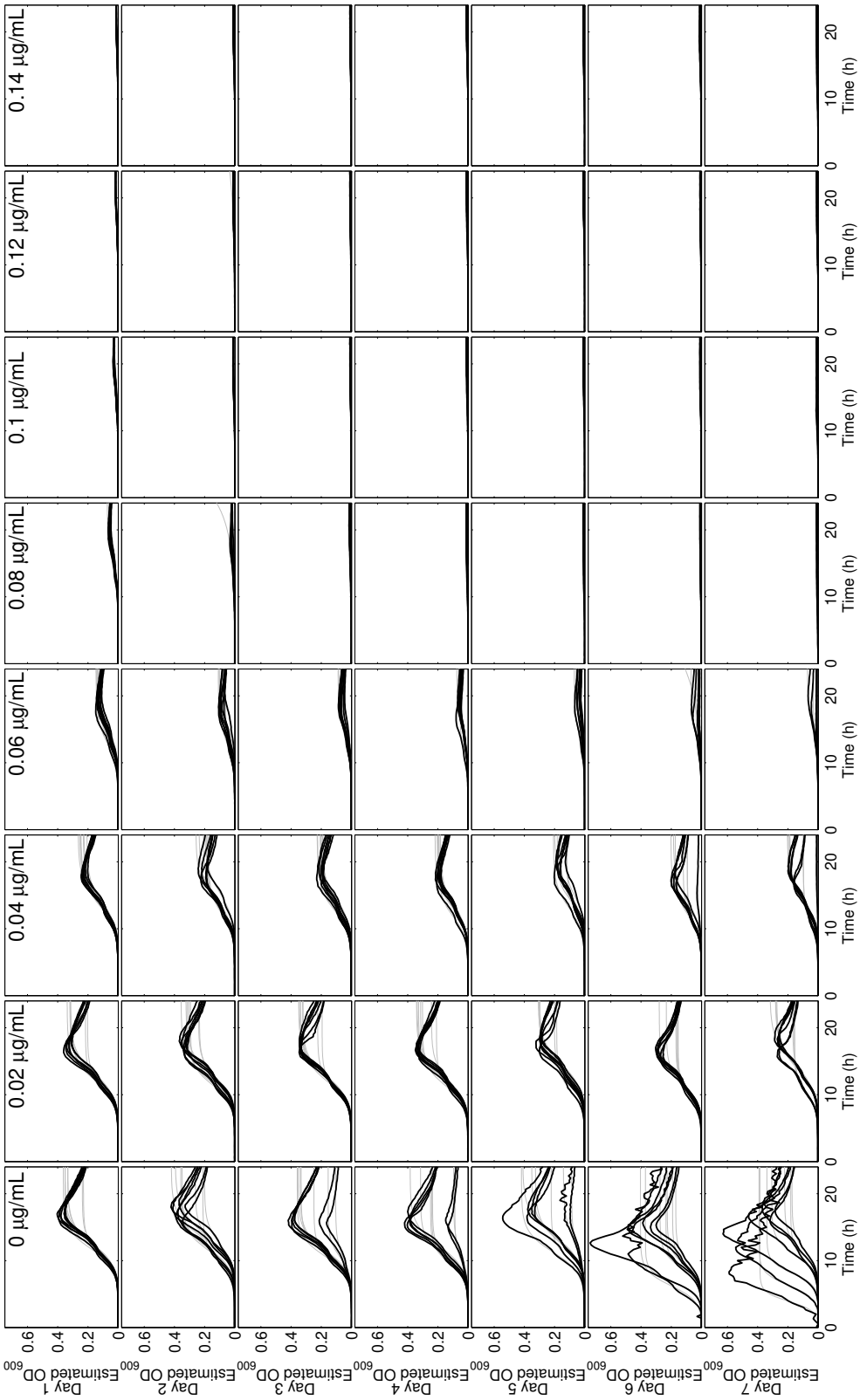

Figure S7. Raw data and model fit for sensitive S strain. Raw optical Density data for Wyl measured every 20min for seven 24h seasons (black). The best fit to data (see methods in main text) used to calculate bacterial fitness is shown in grey. Each column represents the data set for one 24h season and each row the data set for one tetracycline concentration.

bioRxiv preprint doi: https://doi.org/10.1101/810259; this version posted December 20, 2019. The copyright holder for this preprint (which was not certified by peer review) is the author/funder, who has granted bioRxiv a license to display the preprint in perpetuity. It is made available under aCC-BY-NC-ND 4.0 International license.

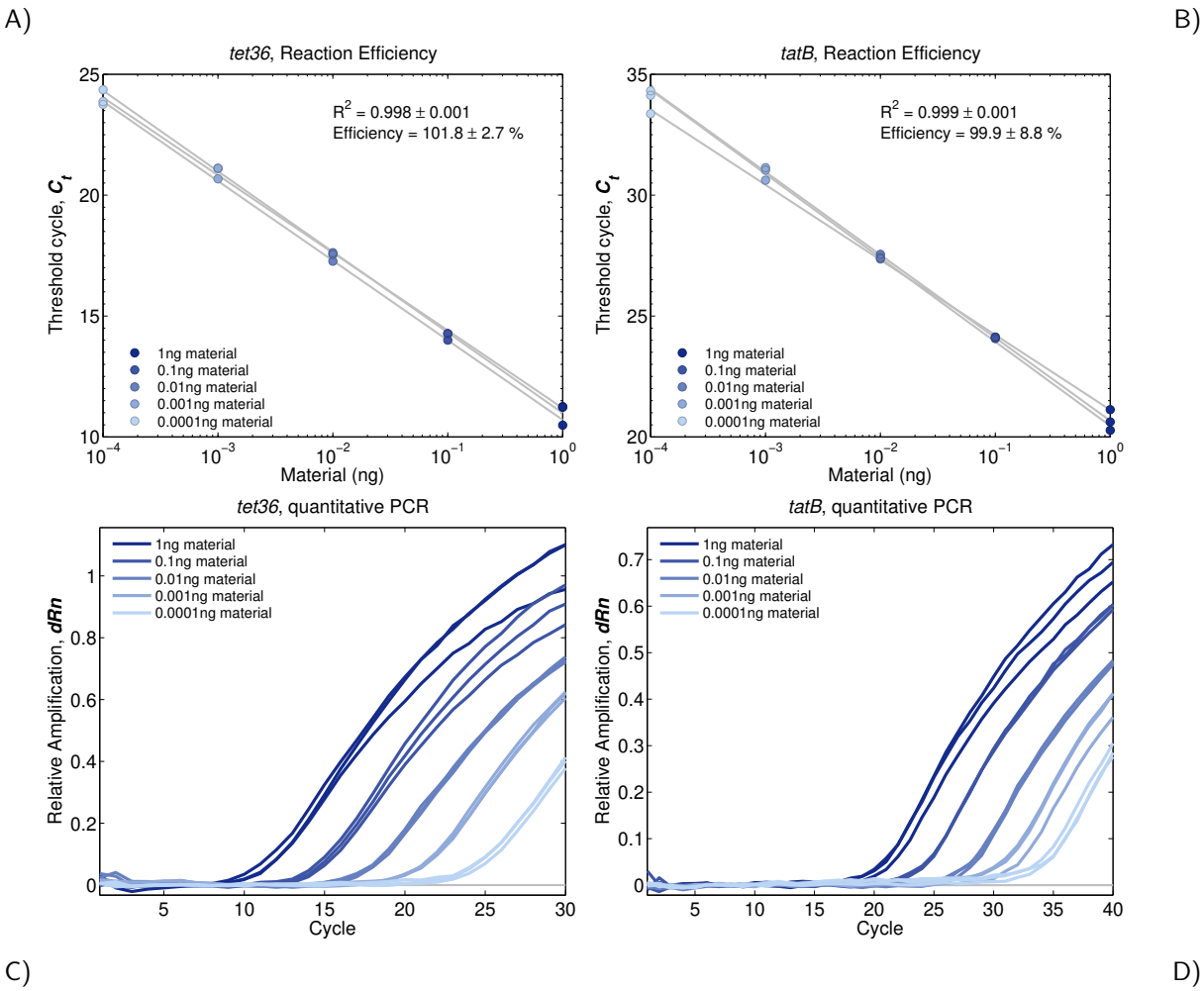

FIGURE S8. Quantitative PCR calibration curves for *tet(36)* and *tatB*. Reaction efficiency for the set of primers and probes listed in the 'methods' section for *tet(36)* (A) and *tatB*. The efficiency was calculated as $E_f = 10^{-1/Slope} - 1$, and the slope term calculated by fitting a linear model to qPCR threshold cycle (C_t) data. The mean ± standard deviation for the coefficient of determination R^2 and efficiency are shown in the figures. The amplification curves for each reaction are shown in C) and D), respectively.